Low field domain wall dynamics in artificial spin-ice basis structure

J. Kwon, S. Goolaup, G. J. Lim, I. S. Kerk, C. H. Chang, K. Roy, and W. S. Lew

Citation: Journal of Applied Physics **118**, 163907 (2015); doi: 10.1063/1.4934733
View online: http://dx.doi.org/10.1063/1.4934733
View Table of Contents: http://scitation.aip.org/content/aip/journal/jap/118/16?ver=pdfcov
Published by the AIP Publishing

Low field domain wall dynamics in artificial spin-ice basis structure

J. Kwon,[1,2] S. Goolaup,[1] G. J. Lim,[1] I. S. Kerk,[1] C. H. Chang,[2,a)] K. Roy,[3] and W. S. Lew[1,b)]
[1]*School of Physical and Mathematical Sciences, Nanyang Technological University, 21 Nanyang Link, Singapore 637371*
[2]*School of Electrical and Electronic Engineering, Nanyang Technological University, 50 Nanyang Avenue, Singapore 639798*
[3]*School of Electrical and Computer Engineering, Purdue University, West Lafayette, Indiana 47907, USA*

(Received 7 July 2015; accepted 13 October 2015; published online 29 October 2015)

Artificial magnetic spin-ice nanostructures provide an ideal platform for the observation of magnetic monopoles. The formation of a magnetic monopole is governed by the motion of a magnetic charge carrier via the propagation of domain walls (DWs) in a lattice. To date, most experiments have been on the static visualization of DW propagation in the lattice. In this paper, we report on the low field dynamics of DW in a unit spin-ice structure measured by magnetoresistance changes. Our results show that reversible DW propagation can be initiated within the spin-ice basis. The initial magnetization configuration of the unit structure strongly influences the direction of DW motion in the branches. Single or multiple domain wall nucleation can be induced in the respective branches of the unit spin ice by the direction of the applied field. © *2015 AIP Publishing LLC*.
[http://dx.doi.org/10.1063/1.4934733]

I. INTRODUCTION

The magnetic charges associated with the magnetization orientation in the ferromagnetic network structures provide an emerging platform for the observation of spin-ice phenomena.[1] The artificial magnetic spin-ice structure is attractive for the creation of monopole-antimonopole pair defects at the vertices of the ferromagnetic network structure, paving the way for the observation of the Dirac string.[2] The unit basis of an artificial spin-ice lattice is comprised of three ferromagnetic bars equilaterally symmetric and converging at a vertex.[3] This unit basis gives rise to different artificial spin-ice lattices such as Kagome and Shakti.[4,5] The initial magnetization configuration of a spin-ice basis determines the net magnetic charges at the vertex. The creation of a monopole is determined by the motion of magnetic charge carriers (domain wall (DW)) in the network structure.[6,7] The DW propagation within an artificial spin-ice nanoarray structure has been shown to adopt both a random[8] and non-random[4] walk. This is attributed to the external driving field and geometrical dimensions of the lattice.[9]

To date, the visualization of magnetic monopole and domain wall propagation through the network structure has been via the direct observation of magnetic properties. Magnetoresistance (MR) measurement is useful for characterizing the spin properties of ferromagnetic nanostructures.[10,11] The detection of a MR signal from the artificial spin-ice may provide an insight into the unique magnetization dynamics in the lattice structure.[12,13] The DW nucleation and motion in the network structure occur at a field much lower than the saturation field. As such, an understanding of low field DW dynamics in an artificial spin-ice lattice is crucial for the magnetization reversal process. In this work, our MR measurement of a unit spin-ice structure reveals that the DW creation and trajectory can be controlled via low field.[14] A transverse DW (TDW) can be created in the selected branches of the spin-ice basis upon application of a low sweeping magnetic field. The advantage of a low sweeping field on the spin-ice basis is to prevent the annihilation of the DWs and the creation of a vortex at the vertex. In our experiment, the interaction of the TDW with the edge defect at the junction leads to a compressed bound state rather than the creation of a vortex or DW annihilation.[15] The bound state dissociates into the vertex and TDW as the field is relaxed.

II. RESULTS AND DISCUSSION

Fig. 1(a) shows the scanning electron microscopy (SEM) image of the basic unit of a spin-ice structure. A Ta(5 nm)/$Ni_{80}Fe_{20}$(10 nm)/Ta(5 nm) thin film structure was grown on a silicon substrate using a sputtering deposition technique and the thin film was patterned by electron beam lithography (EBL). The spin-ice basis consists of the interconnected nanowires of width 100 nm and length 800 nm, with a separation angle of $\theta = 120°$ between each branch, as schematically shown in Fig. 1(b). The nanowire geometrical dimensions ensure that only TDWs are stable and the TDW does not undergo any Walker breakdown.[16,17] Additionally, in our experiment there is a component of the magnetic field perpendicular to the length of the individual branches 2 and 3, which not only locks the chirality of the TDWs but also prohibits them from undergoing a Walker breakdown. Electrical contacts comprised of Ta(5 nm)/Cu(100 nm)/Au(20 nm) are patterned at the end of each nanowire branch of the spin-ice basis. Prior to each MR measurement, the initial magnetization configuration was set by saturating the magnetization along the positive x-axis ($\theta = 0°$) with an external field of 2 kOe and then reducing the field to zero.

a)Electronic mail: echchang@ntu.edu.sg
b)Electronic mail: wensiang@ntu.edu.sg

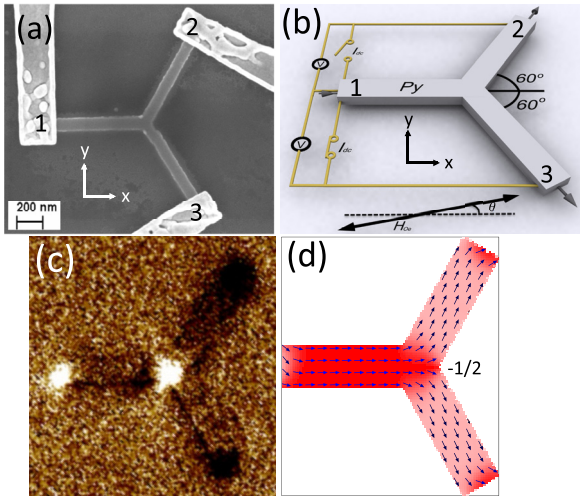

FIG. 1. (a) Scanning electron microscopy (SEM) image of a fabricated spin-ice basis (triple-branch nanowire network) device with electrical contacts. The electrical terminals are labelled as 1, 2, and 3. (b) Illustration of electrical setup for MR measurement, where θ is the angle between the applied field and the x-axis. (c) Magnetic force microscopy of the initial magnetization (remnant) state of a nanowire network system. This configuration is achieved by applying a large external field along the horizontal direction ($\theta = 0°$) and reducing the field to zero. (d) Simulated initial magnetization configuration as obtained by micromagnetic simulation. The spin in the network system follows the geometrical contour of the structure and points along the $+x$-axis orientation.

Fig. 1(c) shows the magnetic force microscopy (MFM) image of the initial magnetization configuration of the structure, with bright and dark contrast at the branch tip and intersection. A simulated initial magnetization state (remnant state) of the network structure is shown in Fig. 1(d) for comparison. The micromagnetic simulation was carried out by using the object oriented micromagnetic framework (OOMMF) program,[18] and the chosen simulation parameters for the $Ni_{80}Fe_{20}$ thin film are saturation magnetization, $M_s = 860 \times 10^3$ A/m, exchange constant, $A = 1.3 \times 10^{-11}$ J/m, anisotropy constant, $K = 0$ and damping constant $\alpha = 0.5$. A unit cell size of $5 \times 5 \times 5\,\text{nm}^3$ was used. The remnant state is characterized by all spins following the geometrical contour of the respective nanowires, with a general component pointing towards the $+x$-orientation. The net magnetic charge distribution in the structure gives rise to the magnetic contrast as seen in the MFM image of Fig. 1(c). At the junction, spins along branch 1 point towards the junction, while spins along both branches 2 and 3 point away from the junction. This leads to a resultant net negative charge at the junction as indicated by the bright contrast of the MFM image. Fig. 1(d) is consistent with the MFM image in Fig. 1(c), where the ends of branches 2 and 3 have a similar dark contrast (positive charge). The net charges in the structure determine the spin component direction along the length of each wire. At the bifurcation in Fig. 1(d), the magnetic configuration gives rise to a $-1/2$ edge defect at the right hand edge of the junction.

MR measurement was first performed using a two-probe technique, while sweeping the magnetic field along the y-axis, ($\theta = 90°$) with reference to branch 1. A constant current of 300 μA, which translates into a current density of $J = 3 \times 10^7$ A/cm^2, was used for all MR measurements. The applied magnetic field was swept from -280 Oe to $+280$ Oe (blue), and from $+280$ Oe to -280 Oe (red), as shown in the MR curve in Fig. 2. The MR as measured between branches 1 and 3 is shown in Fig. 2(a). The MR curve displays the characteristic of a transverse MR profile, with a peak resistance of 468.1 Ω at remnance.[19] This MR behavior is consistent with the magnetization reversal via spin rotation within the structure. For a MR response measured between branches 1 and 2, a different trend is observed as seen in Fig. 2(b). As the field is swept from negative to positive, an abrupt increase in resistance ($\Delta R \sim 0.04$ Ω) is noted at $+79$ Oe in the MR curve. The general trend of the curve is, however, similar to that of the transverse MR. As the field is swept from positive to negative, the curve follows the conventional transverse MR curve. An abrupt decrease in the resistance ($\Delta R \sim 0.08$ Ω) is observed at -258 Oe. The abrupt change in resistance may be due to the nucleation and expulsion of DW within the structure.

To gain a better understanding of the reversal process, micromagnetic simulation was performed. Fig. 2(c) shows

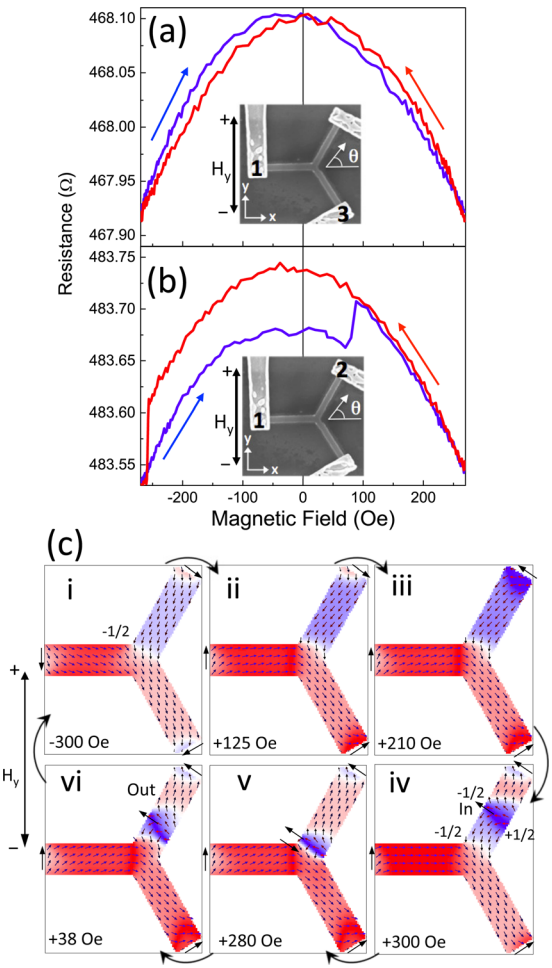

FIG. 2. Low field magnetoresistance as the field is swept within the range of -280 Oe to $+280$ Oe along the y-axis, as measured between the terminals: (a) terminal 1 to terminal 3; (b) terminal 1 to terminal 2. (c) Simulated low field spin configurations of the network structure as the field is swept along the y-axis. The field range is kept between -300 Oe and $+300$ Oe. Simulated spin configurations of the network structure as the external field along the y-axis introduces a TDW in branch 2.

the simulated spin configurations as the field is applied along $\theta = 90°$. The simulation was carried out from the initial magnetization configuration of one-in and two-out, as shown in Fig. 1(d), and follows the same field cycle as the MR measurements. By sweeping the field from negative to positive and setting the field to −300 Oe from the initial configuration, the spins align along the $-y$-axis, with the two-in and one-out configuration, as shown in Fig. 2(c-i). In this configuration, the −1/2 edge defect at the junction has shifted to the top of the junction. As the field increases towards the $+y$ orientation, the spins at the end of branches 1 and 3 flip to align with the field direction. Further increasing the external field induces the spin re-orientation at the end of branch 2. As the field strength is reduced from +300 Oe, TDW is nucleated at the end of branch 2. The transverse component of the TDW is determined by the spin configuration at the end of the nanowire.[20] The nucleated TDW propagates against the field direction towards the junction, as shown in Fig. 2(c-iv). The TDW propagation in the structure tends to recover the initial net charge distribution of the one-in and two-out configuration, as shown in Fig. 1(d). As the TDW moves to the bifurcation, the −1/2 edge defect of the TDW is along the same edge as the −1/2 defect at the junction. Due to the repulsive nature of like topological charges,[21] as the external field is increased, the interaction of the TDW with the vertex leads to the formation of a bound state. This bound state is pinned at the junction and cannot move through the bifurcation. Consequently, the TDW from the end of branch 2 is compressed at the junction, as shown in Fig. 2(c-v) and the TDW trajectory is confined within branch 2 only. This is in contrast to the previously reported results that the TDW transforms into a vortex at the junction.[22] As the field is decreased, the bound state separates into the vertex and TDW. This results in the reversible motion of the TDW within branch 2 at low field. As the field is increased from −300 Oe towards $+H_y$, the re-orientation of spins at the end of branch 2 is observed.

For fields applied from +300 Oe to −300 Oe, starting from the initial configuration, the reversal process is similar except that the TDW is nucleated in branch 3. This is attributed to the symmetry and the position of the −1/2 defect does not undergo any magnetization switching under low field conditions.

The simulation results are consistent with our MR measurements. For branches 1 and 3, where only spin rotation is observed, the MR curve is symmetrical. The presence of a TDW in branch 2 potentially explains the jump in resistance as observed in the measured MR. The MR measured between terminals 2 and 3 for fields applied along the y-axis is shown in Fig. 3(a). The MR curve indicates the characteristics of a longitudinal MR, characterized by two minima ($R \sim 579.06\ \Omega$) at ±200 Oe. As the field is increased from the maximum negative, we observed that the resistance starts to decrease prior to the external field reaching zero. This is due to the alignment of spins within the structure along the branch axis as the external field is reduced to zero. Further increase in the external field leads to a gradual drop of the resistance until the local minimum is reached at 200 Oe. The resistance then increases via two sudden jumps to reach the maximum field resistance. As

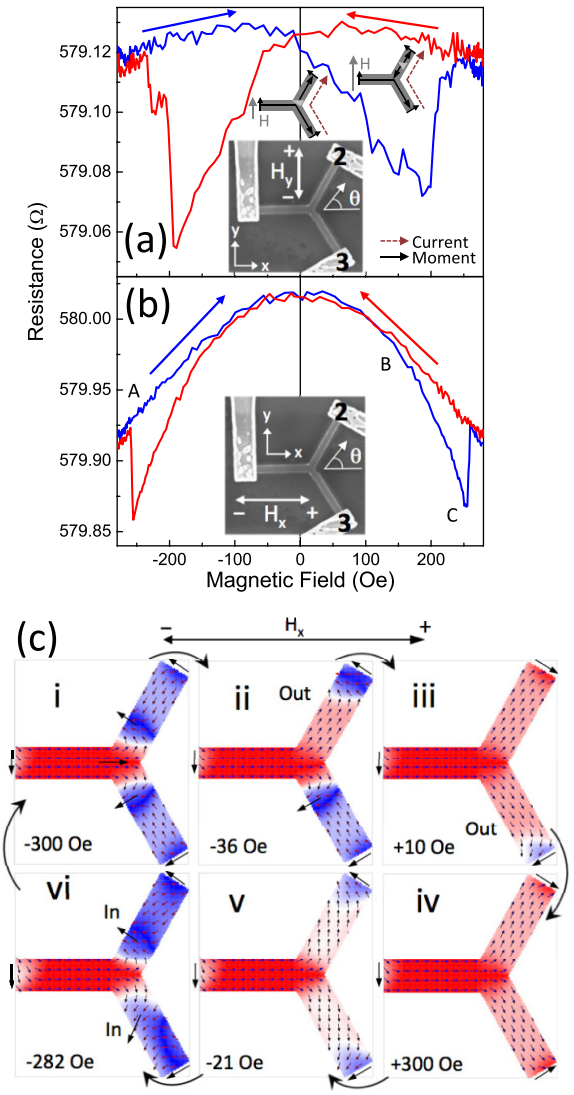

FIG. 3. Magnetoresistance measurements between terminals 2 and 3 as the field is swept along the (a) y-axis and (b) x-axis. Insets (illustrations) in the figure show the MR effect corresponding to the current direction on the device with respect to the field angle $\theta = 90°$ (y-axis) and at $\theta = 0°$ (x-axis). (c) Simulated spin configurations of the network structure as the field along the x-axis introduce the TDWs in branches 2 and 3.

seen in Fig. 2(c), within the field range investigated, only branch 2 switches its magnetization orientation and this is achieved via TDW nucleation and propagation. The gradual decrease of the resistance in the curve is attributed to the nucleation and propagation of the TDW in the MR plot. The two jumps in the resistance are potentially attributed to the ejection of the TDW from branch 2 and the spin re-orientations at the ends of the branch.

In the following part, the MR is measured between terminals 2 and 3, with the field sweeping along the x-axis ($\theta = 0°$) direction, as shown in Fig. 3(b). The measurement reveals the characteristic of a transverse MR with the maximum resistance when the direction of the current is parallel to the magnetic moments along the field direction.[23,24] As the field magnitude decreases from −280 Oe, the MR gradually increases up to the maximum resistance at zero field. The resistance decreases rapidly from +140 Oe to the

minimum at +250 Oe, followed by a sudden increase, as seen by the sequence A, B, and C in Fig. 3(b). The transverse MR follows a $\cos^2\theta$ behavior. However, the MR measured in Fig. 3(b) displays a deviation from this behavior. Interestingly, this is observed for both field sweep orientations. Our simulation results reveal that the reversal process is via the nucleation of the TDWs in both branches 2 and 3 as the field is swept, as shown in Fig. 3(c). As the field is increased from the maximum negative, we note that the motion of the TDW in the individual branches occurs at different field values. This may explain the asymmetric nature of the MR response. The TDW motion in branch 3 induces the lower MR due to the anti-parallel moments to the current. Further increase of the positive field strength causes the flipping of the transverse component spin at the end of branch 3 as shown in Figs. 3(c-iii) and 3(c-iv). As discussed previously, the interaction of the topological charges in the structure leads to the repulsion of the TDW from the respective branches at the bifurcation. As such, at low field, the TDW from branches 2 and 3 do not move through the junction. The sudden increase in resistance ($\Delta R \sim 0.06\ \Omega$) is due to the change of the spin orientation (compressed "V" configuration) at the end of branch 3 along the field direction.[25,26] The process of the TDW nucleation and propagation follows the initial magnetic charge contribution, which leads to the minimization of the total magnetic energy in the system.

III. SUMMARY

In summary, the MR curves reveal that the nucleation and annihilation of the TDW in the spin-ice basis is reflected by sharp jumps in resistance. The nucleation of the TDW in the individual branches of the spin-ice basis is determined by the direction of the applied external field. The TDW behavior at low field is quite different from the TDW evolution at the junction at high field. We observed that the TDW is pinned at the junction and undergoes the contraction/expansion at low field.

ACKNOWLEDGMENTS

The work was supported by a MOE-AcRF Tier 2 Grant (MOE 2013-T2-2-017). Support from a NRF-CRP grant (Non-volatile Logic and Memory Integrated Circuit Devices, NRF-CRP9-2011-01) is also acknowledged.

[1]W. R. Branford, S. Ladak, D. E. Read, K. Zeissler, and L. F. Cohen, Science **335**, 1597 (2012).
[2]E. Mengotti, L. J. Heyderman, A. F. Rodríguez, F. Nolting, R. V. Hügli, and H.-B. Braun, Nat. Phys. **7**, 68 (2010).
[3]A. Pushp, T. Phung, C. Rettner, B. P. Hughes, S.-H. Yang, L. Thomas, and S. S. P. Parkin, Nat. Phys. **9**, 505 (2013).
[4]K. Zeissler, S. K. Walton, S. Ladak, D. E. Read, T. Tyliszczak, L. F. Cohen, and W. R. Branford, Sci. Rep. **3**, 1252 (2013).
[5]I. Gilbert, G.-W. Chern, S. Zhang, L. O'Brien, B. Fore, C. Nisoli, and P. Schiffer, Nat. Phys. **10**, 670 (2014).
[6]P. Mellado, O. Petrova, Y. Shen, and O. Tchernyshyov, Phys. Rev. Lett. **105**, 187206 (2010).
[7]Y. Shen, O. Petrova, P. Mellado, S. Daunheimer, J. Cumings, and O. Tchernyshyov, New J. Phys. **14**, 035022 (2012).
[8]D. M. Burn, M. Chadha, S. K. Walton, and W. R. Branford, Phys. Rev. B **90**, 144414 (2014).
[9]S. K. Walton, K. Zeissler, D. M. Burn, S. Ladak, D. E. Read, T. Tyliszczak, L. F. Cohen, and W. R. Branford, New J. Phys. **17**, 013054 (2015).
[10]M. Tanaka, E. Saitoh, H. Miyajima, T. Yamaoka, and Y. Iye, Phys. Rev. B **73**, 052411 (2006).
[11]S. Lepadatu and Y. B. Xu, IEEE Trans. Magn. **40**, 2688 (2004).
[12]E. Saitoh, M. Tanaka, H. Miyajima, and T. Yamaoka, J. Appl. Phys. **93**, 7444 (2003).
[13]S. Ladak, D. E. Read, G. K. Perkins, L. F. Cohen, and W. R. Branford, Nature Phys. **6**, 359 (2010).
[14]O. Tchernyshyov and G.-W. Chen, Phys. Rev. Lett. **95**, 197204 (2005).
[15]M. Hayashi, L. Thomas, R. Moriya, C. Rettner, and S. S. Parkin, Science **320**, 209 (2008).
[16]Y. Nakatani, A. Thiaville, and J. Miltat, J. Magn. Magn. Mater. **290**, 750 (2005).
[17]M. Hayashi, L. Thomas, Ya. B. Bazaliy, C. Rettner, R. Moriya, X. Jiang, and S. S. P. Parkin, Phys. Rev. Lett. **96**, 197207 (2006).
[18]M. J. Donahue and D. G. Porter, See http://math.nist.gov/oommf/, for OOMMF User's Guide, NIST, 2002.
[19]M. Tanaka, E. Saitoh, H. Miyajima, and T. Yamaoka, J. Appl. Phys. **99**, 08G314 (2006).
[20]R. D. McMichael and M. J. Donahue, IEEE Trans. Magn. **33**, 4167 (1997).
[21]L. Thomas, M. Hayashi, R. Moriya, C. Rettner, and S. Parkin, Nat. Commun. **3**, 810 (2012).
[22]C. Murapaka, P. Sethi, S. Goolaup, R. Maddu, Y. Chen, S. H Leong, and W. S. Lew, Appl. Phys. Express **7**, 113003 (2014).
[23]J.-E. Wegrowe, D. Kelly, A. Franck, S. E. Gilbert, and J.-Ph. Ansermet, Phys. Rev. Lett. **82**, 3681 (1999).
[24]H. Corte-Leon, V. Nabaei, A. Manzin, J. Fletcher, P. Krzysteczko, H. W. Schumacher, and O. Kazakova, Sci. Rep. **4**, 6045 (2014).
[25]H. T. Zeng, D. Read, L. O'Brien, J. Sampaio, E. R. Lewis, D. Petit, and R. P. Cowburn, Appl. Phys. Lett. **96**, 262510 (2010).
[26]L. J. Chang, Y. D. Yao, P. Lin, and S. F. Lee, IEEE Trans. Magn. **47**, 2519 (2011).